Radboud Universiteit

From Fermi resonance and string pendulum to Van der Waals heterostructures

Mikhail Katsnelson

IMM
Institute for Molecules and Materials

Infrared optics of molecules and crystals

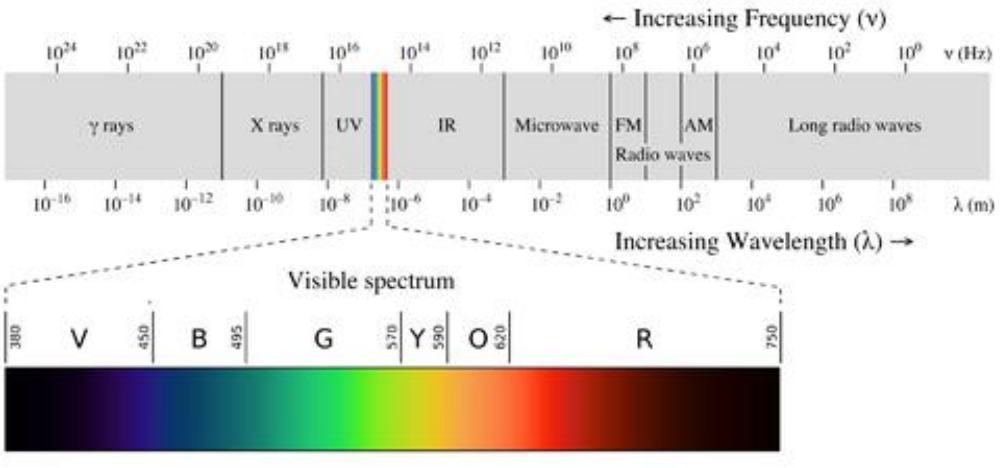

Electromagnetic radiation (Wiki)

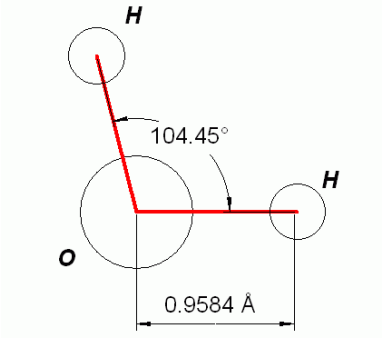

Geometry of water molecule

$1\ \text{Å} = 10^{-10}\ \text{m}$

Thousands of times smaller than wavelength of visual light

For infrared and visual light: wavelength is much larger than interatomic distance, electric field can be considered as homogeneous

$$\mathbf{E}(t) = \mathbf{E}\cos\omega t$$

Interaction with electric dipole moment is the main effect

$$V = -\mathbf{d}\mathbf{E}(t)$$

Infrared optics of molecules and crystals II

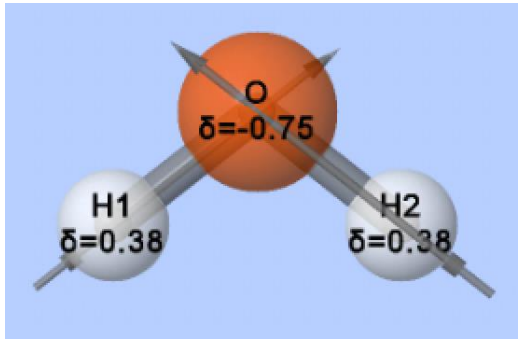

Charge transfer in molecules induces dipolar moments which can oscillate

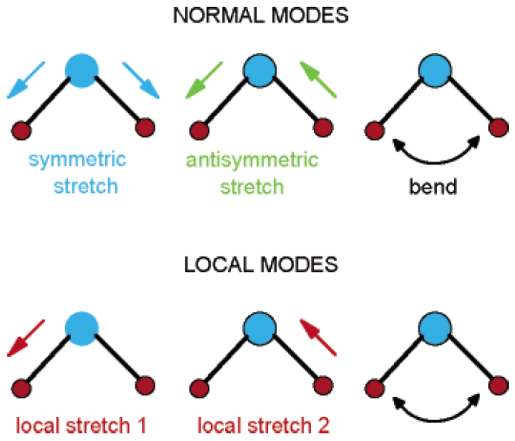

FIGURE 1. Normal and local modes of H_2O: top, normal modes—symmetric stretch, antisymmetric stretch, bend; bottom, local stretch modes.

Kellman & Ting, Acc. Chem. Res. 2007, 40, 243

Symmetry analysis (E. Wigner): for some modes average dipole moment is nonzero, leads to IR adsorption/emission. For some modes it is zero but they are active in the second-order (Raman effect, a.k.a. combination scattering)

Raman effect

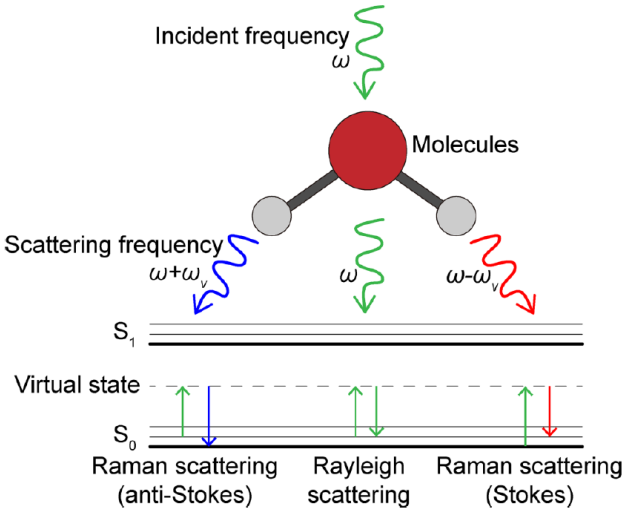

Lin et al, J. Appl. Phys. 129, 191101 (2021)

Quantum theory of scattering
(Kramers-Heisenberg formula)

$$\frac{d\sigma}{do'} = \frac{\omega\omega\prime^3}{\hbar^2 c^4}\left|\sum_n \left\{\frac{(\vec{d}_{fn}\vec{e}'^*)(\vec{d}_{ni}\vec{e})}{\omega_{ni}-\omega-i\delta}+\frac{(\vec{d}_{fn}\vec{e})(\vec{d}_{ni}\vec{e}'^*)}{\omega_{ni}+\omega-i\delta}\right\}\right|^2_{\delta\to+0}$$

$$\omega_{ni} = \frac{E_n - E_i}{\hbar}$$

For scattered light

$$\omega' = \omega + \frac{E_i - E_f}{\hbar}$$

The frequency of scattered light $\omega' = \omega \pm \omega_\lambda$

ω_λ frequencies of Raman active vibration modes

Raman effect: Classical interpretation

From Maxwell electrodynamics: refraction index

$$n^2(\omega) = \varepsilon(\omega)$$

Suppose that dielectric function is modulated by atomic vibrations:

$$\varepsilon(t) = \varepsilon_0(1 + \alpha \cos \omega_1 t)(\alpha \ll 1)$$

Then, we will have combined frequencies of light since

$$\cos \omega t \cos \omega_1 t = \frac{\cos(\omega + \omega_1)t + \cos(\omega - \omega_1)t}{2}$$

Combination scattering, Mandelstam and Landsberg, simultaneously with Raman and Krishnan

Fermi resonance

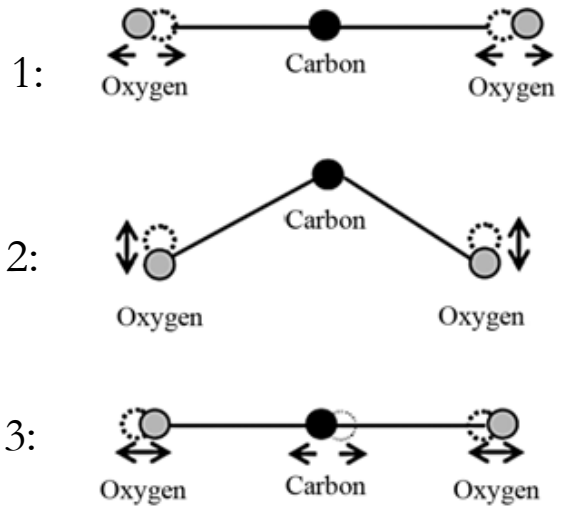

CO_2 molecule: symmetry analysis predicts *one* Raman-active mode, ν_1 without average dipole moment, others are IR active

Experimentally: four Raman lines, two strong and two weak

Fermi explanation: accidental (almost) degeneracy $\omega_1 \approx 2\omega_2$

IR active modes at 670 and 2350 cm^{-1}

Main Raman lines at 1285 and 1300 cm^{-1}

Close to 670 x 2 = 1340

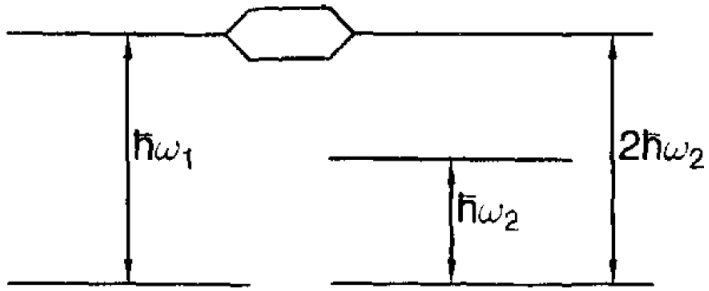

$$E_1 = \hbar\omega_1, \; E_1 = 2\hbar\omega_2$$

almost degenerate

Coupling $V = \lambda x_1 x_2^2$

mixes the states, results in splitting

Phase locking (synchronization)

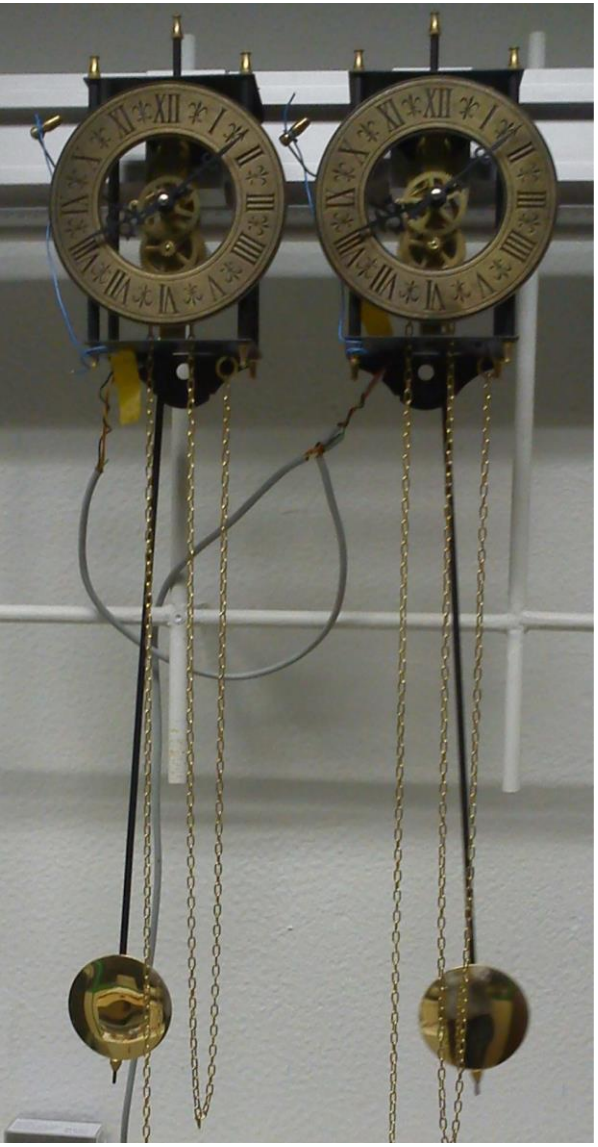

Oliveira & Melo, Sci Rep 2015

Discovered by Huygens, XVII century)

If you have two coupled oscillators with slightly different frequencies they can be synchronized

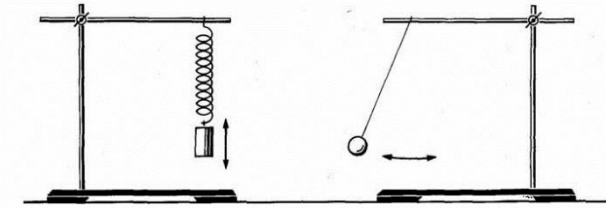

E.g., string pendulum, frequency ratio close to 1:2

Bifurcation of torus (with two incommensurate frequencies) into limit circle (with one common period)

Phase synchronization II

Superposition of two periodic motions: Lissajous figures

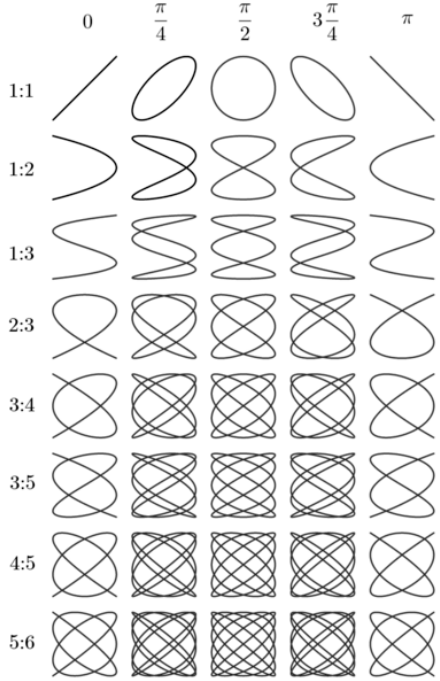

If frequencies are commensurate (their ratio is rational, there is a common Period) the motion is periodic

Usually represented in phase space as tori

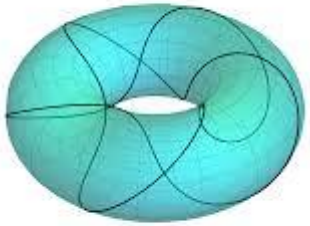

Representing in perpendicular directions

If the ratio is incommensurate the motion id quasiperiodic and trajectory fills the torus

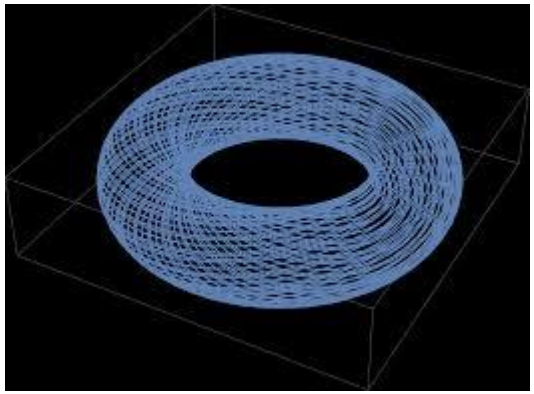

Phase synchronization III

Periodic motion in dissipative systems: limit cycles describing self-oscillation

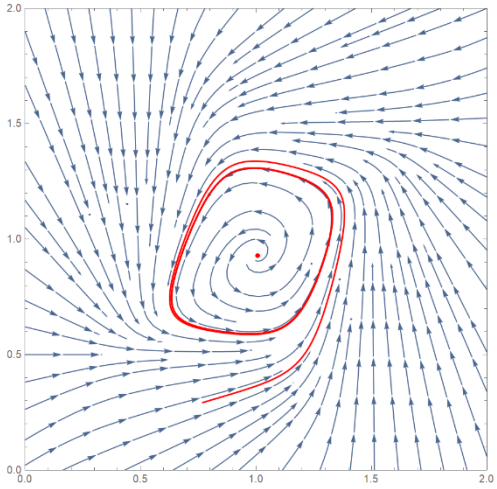

Closed trajectory, asymptotically stable

Everywhere: from electrical engineering to biology

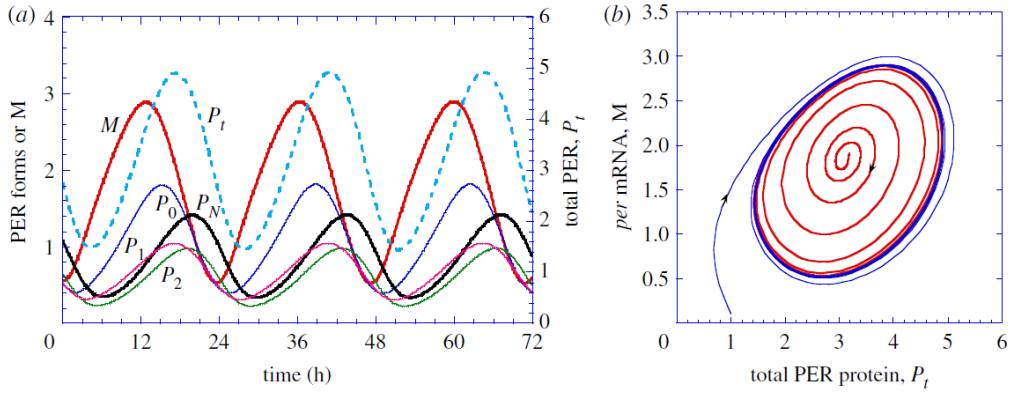

Figure 3. Sustained oscillations in a model for circadian oscillations of the PER protein in *Drosophila*. The oscillations (*a*) correspond to the evolution to a limit cycle (*b*), which is reached regardless of initial conditions. Two different initial conditions lead to the same closed trajectory (from Goldbeter [159]). (Online version in colour.)

Goldbeter A. 2018 *Phil. Trans. R. Soc. A* **376**: 20170376

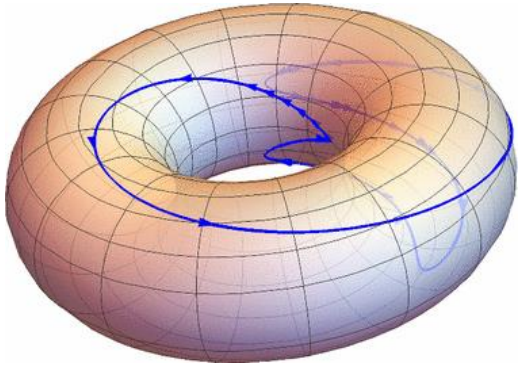

Phase synchronization is a bifurcation of tori to limit cycle

String pendulum

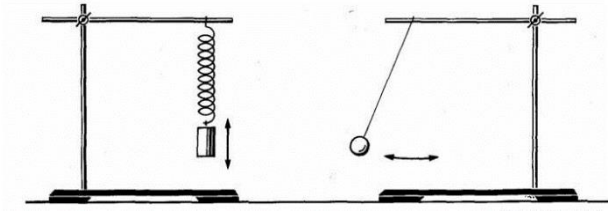

String pendulum, frequency ratio close to 1:2

Classical model of Fermi resonance (much more difficult and rich than quantum)

Stochastic resonance between limit cycles. Spring pendulum in a thermostat

Yu. N. Gornostyrev, D. I. Zhdakhin, and M. I. Katsnel'son
Institute of Metal Physics, Ural Branch of the Russian Academy of Sciences, 620219 Ekaterinburg, Russia

A. V. Trefilov
Russian Science Center "Kurchatov Institute," 123182 Moscow, Russia

(Submitted 18 March 1999)
Pis'ma Zh. Éksp. Teor. Fiz. **69**, No. 8, 585–589 (25 April 1999)

$$L = 1/2(\dot{x}^2 + \dot{y}^2) - V(x,y), \qquad (1)$$

$$V = \frac{k}{2}(r-l)^2 + gr(1-\cos\phi)$$

$$= 1/2\left\{ \omega_0^2[x^2 + (y+1)^2] + 2(\Omega_0^2 - \omega_0^2)\sqrt{x^2 + (y+1)^2} - 2\Omega_0^2(y+1) + \frac{(\Omega_0^2 - \omega_0^2)}{\omega_0^2} \right\},$$

$$\omega_0 = \sqrt{k} \text{ and } \Omega_0 = \sqrt{g/l} \qquad \omega_0 = 2\Omega_0 + \Delta,\ \Delta \ll \Omega_0$$

String pendulum II

Thermal noise

$$\ddot{x}+2\gamma\dot{x}+\frac{\partial V}{\partial x}=f_x(t),$$

$$\ddot{y}+2\Gamma\dot{y}+\frac{\partial V}{\partial y}=f_y(t),$$

$$\langle f_x(t)f_x(t')\rangle=4T\gamma\delta(t-t'),$$

$$\langle f_y(t)f_y(t')\rangle=4T\Gamma\delta(t-t'),$$

$$\langle f_x(t)f_y(t')\rangle=0.$$

Numerics

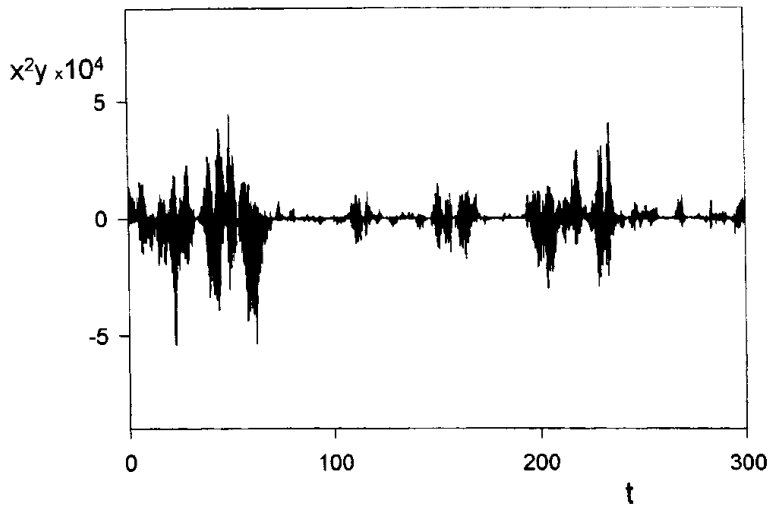

FIG. 1. Typical dependence $x^2(t)y(t)$ in the stationary state with $\Delta=0$, $T=0.025$, $\gamma=0.005$, and $\Gamma=0.005$.

There is an energy transfer from one mode to the other

String pendulum III

$$s(t) = \Omega_0 \int_{t-n\pi/\Omega_0}^{t+n\pi/\Omega_0} x^2(t')y(t')\cos(4\Omega_0 t')dt'$$

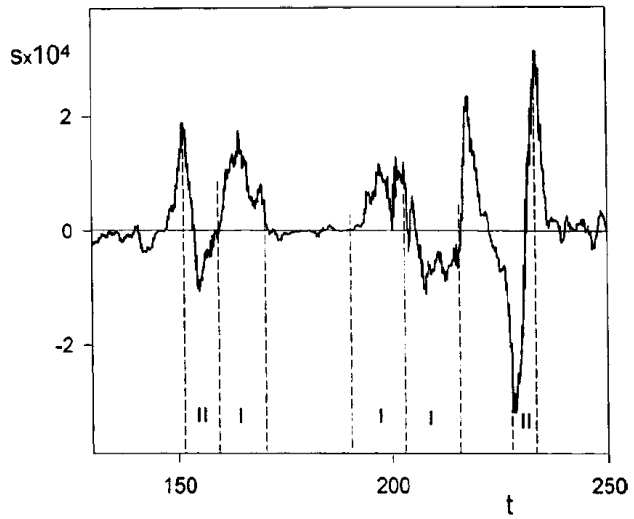

FIG. 2. $s(t)$ (see the expression (4)) for the same parameters as in Fig. 1. The sections corresponding to phase synchronization (limit cycles) are designated by I, and the sections corresponding to fast transitions between limit cycles are designated by II.

Long-term periodicity: what does it mean?

String pendulum IV

Журнал экспериментальной и теоретической физики

Т. 97 *1990* *Вып. 6*

М. И. Кацнельсон, А. В. Трефилов

СИНХРОНИЗАЦИЯ ФОНОННЫХ ЧАСТОТ И КВАЗИСТАТИЧЕСКИЕ СМЕЩЕНИЯ АТОМОВ В КРИСТАЛЛАХ

Coupled fields with cubic nonlinearity uv^2:

$$\ddot{u}+\omega^2(-i\nabla)u+2\gamma(-i\nabla)\dot{u}+\lambda v^2=0,$$

$$\ddot{v}+\Omega^2(-i\nabla)v+2\Gamma(-i\nabla)\dot{v}+2\lambda uv=0,$$

$$u(\mathbf{r},t)=A(\mathbf{r},t)\exp\{i[\mathbf{q}_0\mathbf{r}-\omega(\mathbf{q}_0)t]\}+B(\mathbf{r},t)\exp\{i[\mathbf{q}_0\mathbf{r}+\omega(\mathbf{q}_0)t]\}+\text{к. с.},$$

$$v(\mathbf{r},t)=C(\mathbf{r},t)\exp\{i[\mathbf{q}_0\mathbf{r}+\omega(\mathbf{q}_0)t/2]\}+D(\mathbf{r},t)\exp\{i[\mathbf{q}_0\mathbf{r}-\omega(\mathbf{q}_0)t/2]\}+\text{к. с.}. \quad (2)$$

Separating resonance terms:

$$\frac{\partial A}{\partial t}+\left(\frac{\partial\omega}{\partial\mathbf{q}}\right)_0\nabla A-\frac{i}{4\omega_0}\left(\frac{\partial^2\omega^2}{\partial q_\alpha\,\partial q_\beta}\right)\frac{\partial^2 A}{\partial x_\alpha\,\partial x_\beta}+\gamma_0 A+i\Lambda(C^*)^2=0, \quad (3)$$

$$\frac{\partial C}{\partial t}-\left(\frac{\partial\omega}{\partial\mathbf{q}}\right)_0\nabla C+\frac{i}{2\omega_0}\left(\frac{\partial^2\Omega^2}{\partial q_\alpha\partial q_\beta}\right)_0\frac{\partial^2 C}{\partial x_\alpha\,\partial x_\beta}+\left(\Gamma_0+\frac{i\nu_0}{2}\right)C-4i\Lambda A^*C^*=0. \quad (4)$$

$$\omega=2\Omega+\nu\ \ (|\nu|\ll\omega),\ \Lambda\equiv\lambda/2\omega_0$$

String pendulum V

Analysis of these equations show existence of *two* limit cycles with different total phases. Thermal noise induces an (almost) periodic transitions between two these limit cycles

Coming back to the Fermi resonance in string pendulum model

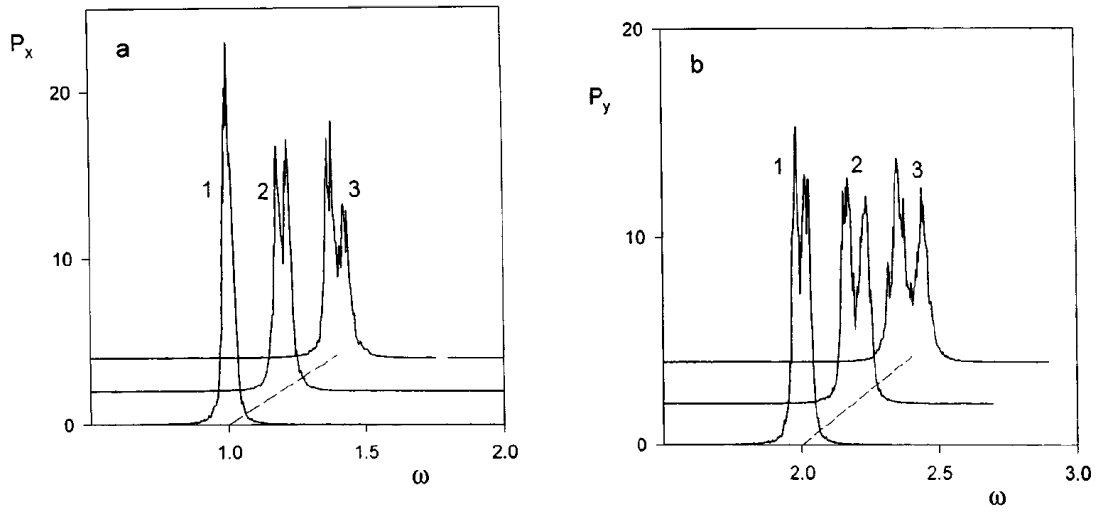

FIG. 4. Spectral densities $P_x(\omega)=|x_\omega|^2$ and $P_y(\omega)=|y_\omega|^2$ normalized to 1 for $\Delta=0$, $\gamma=0.005$, and $\Gamma=0.005$. The curves *1–3* are presented for $T=0.001$, 0.0025, and 0.005, respectively. For convenience the coordinate origin of the curves *2* and *3* is shifted.

Splitting of main frequencies!

Recent development: magnon-phonon resonance in antiferromagnet CoF_2

Impulsive Fermi spin-lattice resonance in antiferromagnetic CoF_2

Thomas W.J. Metzger[1*], Kirill A. Grishunin[1], Chris Reinhoffer[2], Roman M. Dubrovin[3], Atiqa Arshad[4], Igor Ilyakov[4], Thales V.A.G. de Oliveira[4], Alexey Ponomaryov[4], Jan-Christoph Deinert[4], Sergey Kovalev[4], Roman V. Pisarev[3], Mikhail I. Katsnelson[1], Boris A. Ivanov[1], Paul H. M. van Loosdrecht[2], Alexey V. Kimel[1] and Evgeny A. Mashkovich[2]

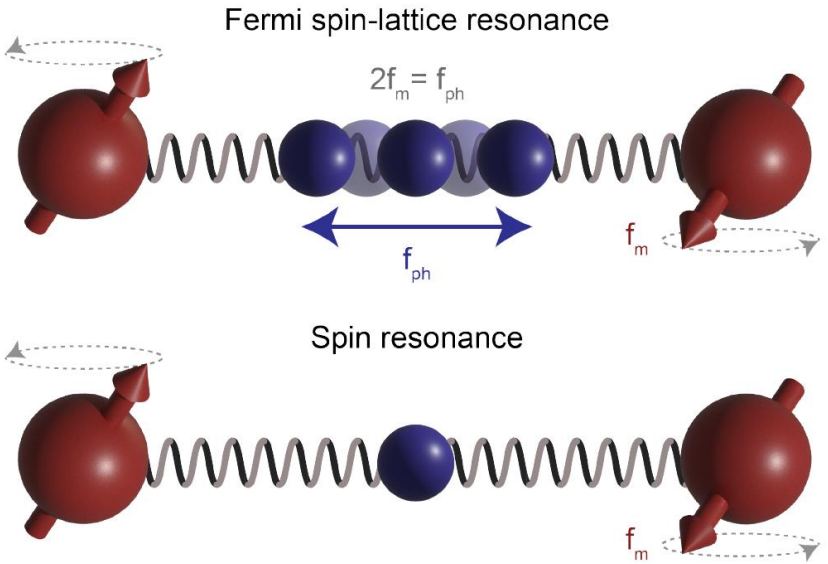

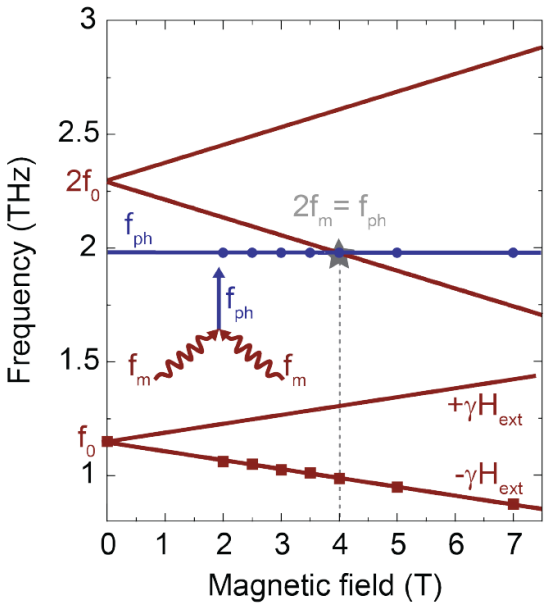

Fig. 1 Sketch of nonlinear spin-lattice dynamics. (a) For $2f_m = f_{ph}$, the Fermi spin-lattice resonance condition is fulfilled and the the nonlinear energy transfer channel between a magnon and a phonon opens. (b) The Frequency tuning by an external magnetic field applied along the antiferromagnetic easy axis. The frequency matching condition is marked by a grey star. The Feynman diagram illustrates the two magnon - one phonon conversion process.

Recent development: magnon-phonon resonance in antiferromagnet CoF_2 II

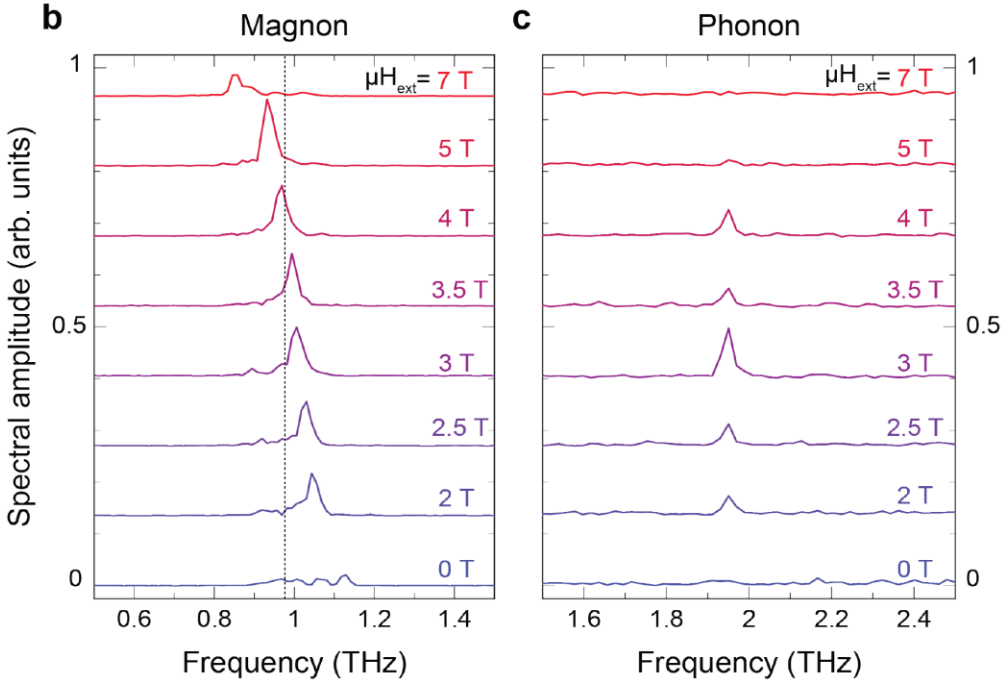

Energy transfer from magnon to phonon mode near the resonance condition

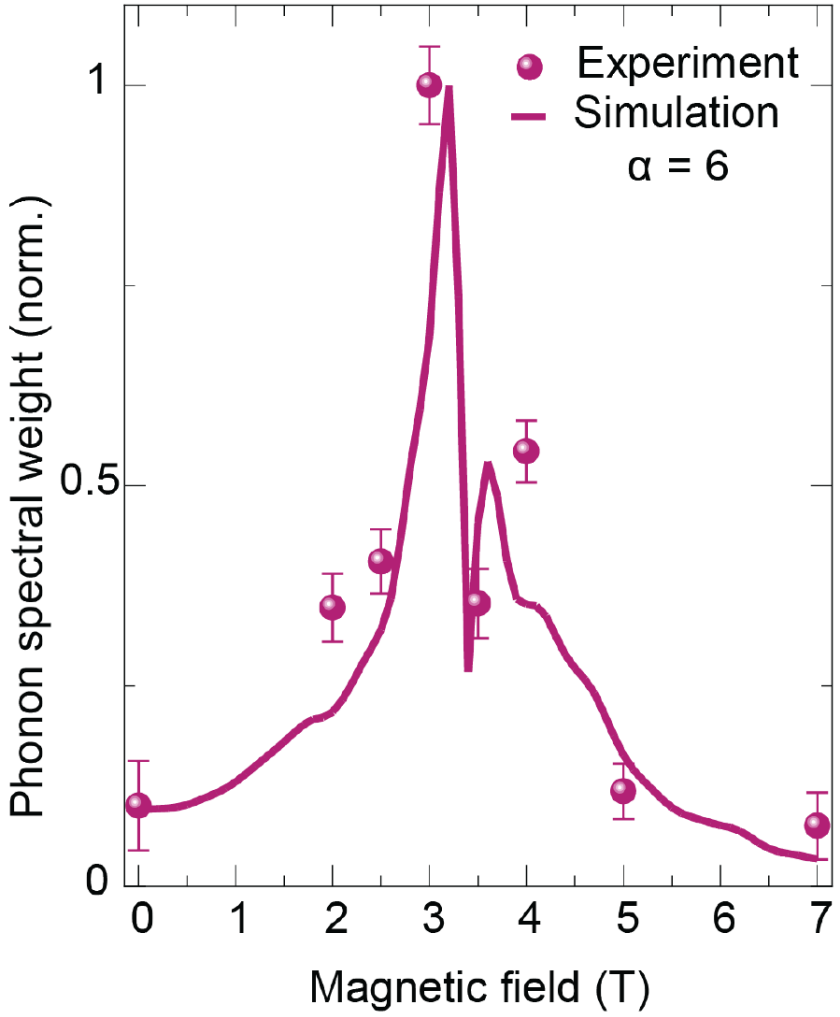

Amplitude of excited phonon signal

Second part: Synchronization in space

Misfit dislocations

One-dimensional dislocations.

I. Static theory

By F. C. Frank and J. H. van der Merwe

H. H. Wills Physical Laboratory, University of Bristol

(*Communicated by N. F. Mott, F.R.S.—Received 22 December 1948—Revised 25 March 1949—Read 19 May 1949*)

$$V_N = \tfrac{1}{2}\mu \sum_{n=0}^{N-1} (x_{n+1} - x_n + a - b)^2 + \tfrac{1}{2} W \sum_{n=0}^{N-1} (1 - \cos 2\pi x_n/a)$$

Energy of interlayer interaction (second term) wants that interatomic distances are equal but then one pays for the energy of elastic deformation (the first term)

Interface of different semiconductors (e.g. PbTe/PbSe)

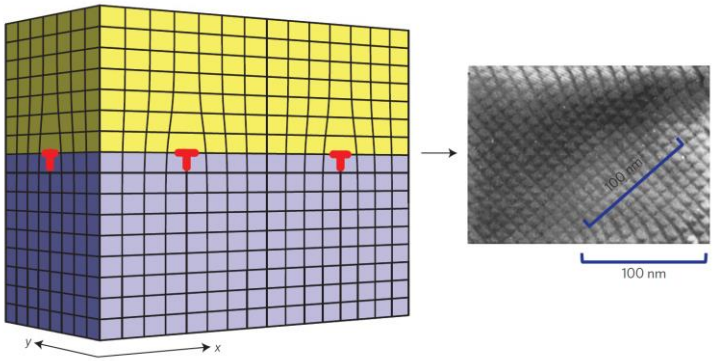

Tang & Fu, Nature Phys. 10, 964 (2014)

Very roughly: When $W > \mu(b-a)^2$ then two layers will be mostly commensurate, and the whole misfit will be concentrated via narrow 'solitons', and in the opposite limit the system will not even try To reach synchronization of periods, that is, commensurability

Commensurate – incommensurate transition is expected!

Van der Waals Heterostructures

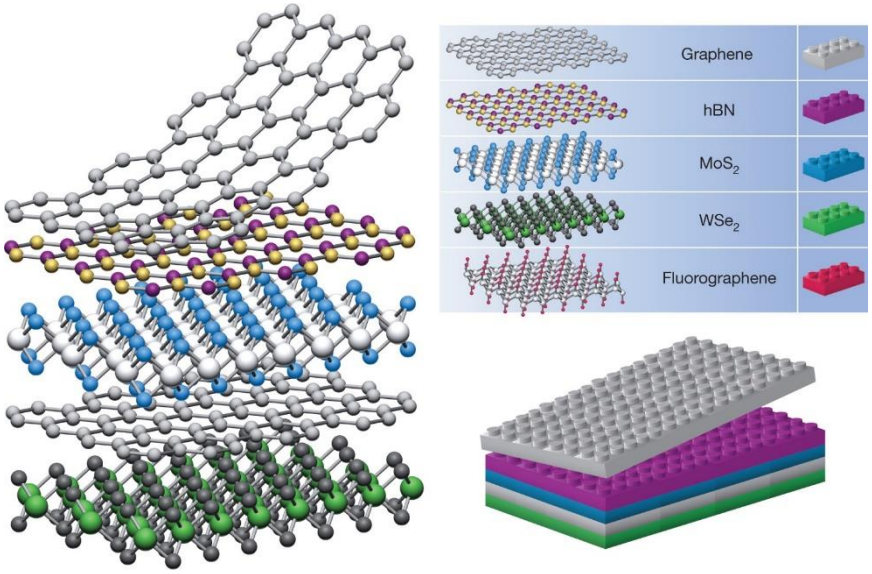

"Van der Waals heterostructures"
Geim & Grigorieva, Nature 2013

Combination of 2D materials create new physical systems and open ways for new application

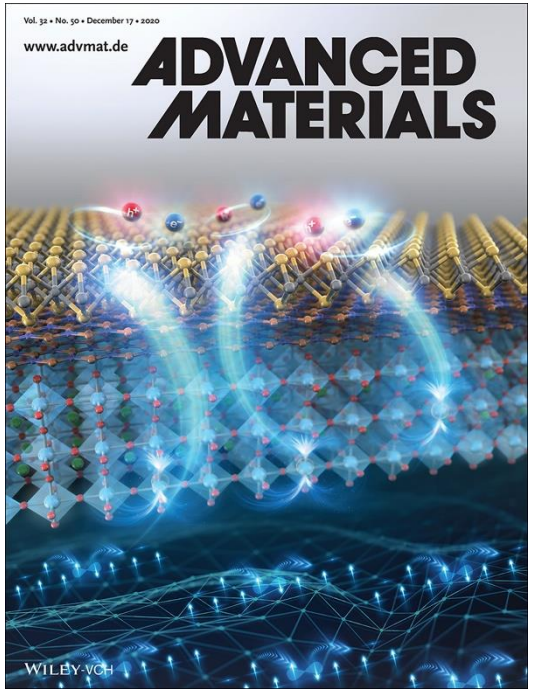

Twisted bilayer graphene: Flat bands and all that

Correlated insulator behaviour at half-filling in magic-angle graphene superlattices

Yuan Cao[1], Valla Fatemi[1], Ahmet Demir[1], Shiang Fang[2], Spencer L. Tomarken[1], Jason Y. Luo[1], Javier D. Sanchez-Yamagishi[2], Kenji Watanabe[3], Takashi Taniguchi[3], Efthimios Kaxiras[2,4], Ray C. Ashoori[1] & Pablo Jarillo-Herrero[1]

Unconventional superconductivity in magic-angle graphene superlattices

Yuan Cao[1], Valla Fatemi[1], Shiang Fang[2], Kenji Watanabe[3], Takashi Taniguchi[3], Efthimios Kaxiras[2,4] & Pablo Jarillo-Herrero[1]

5 APRIL 2018 | VOL 556 | NATURE | 43

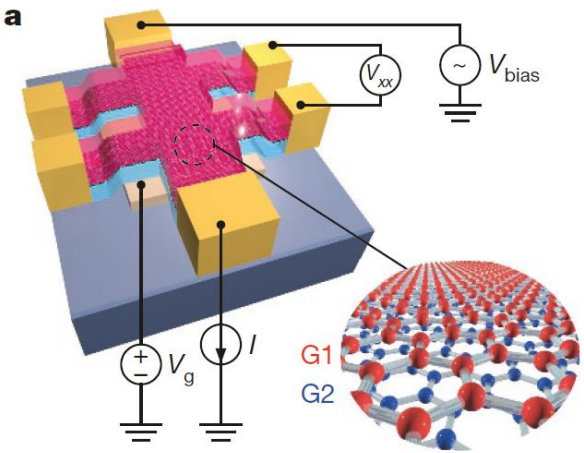

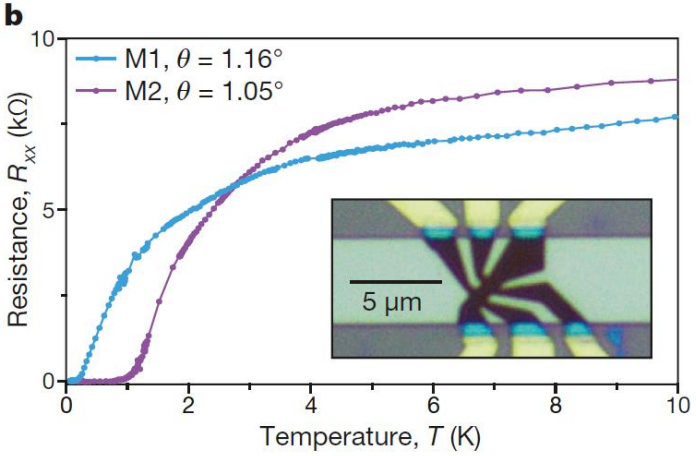

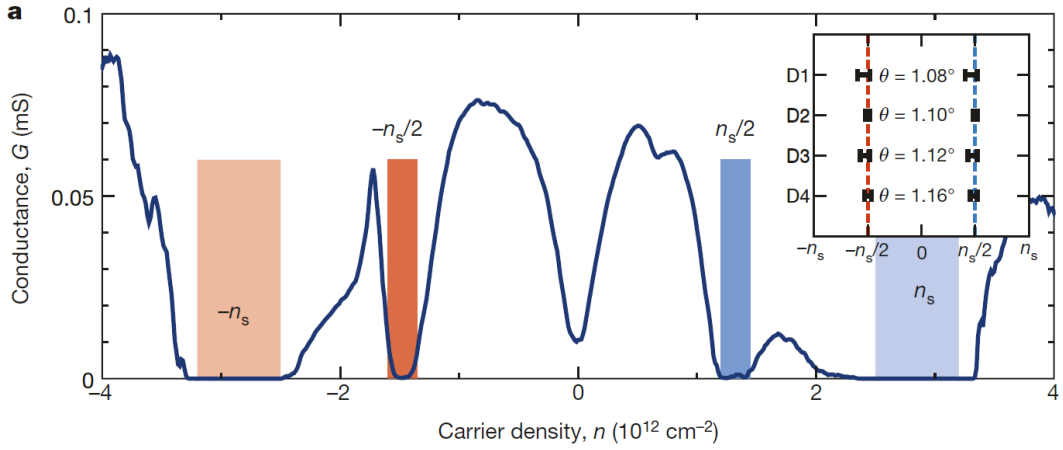

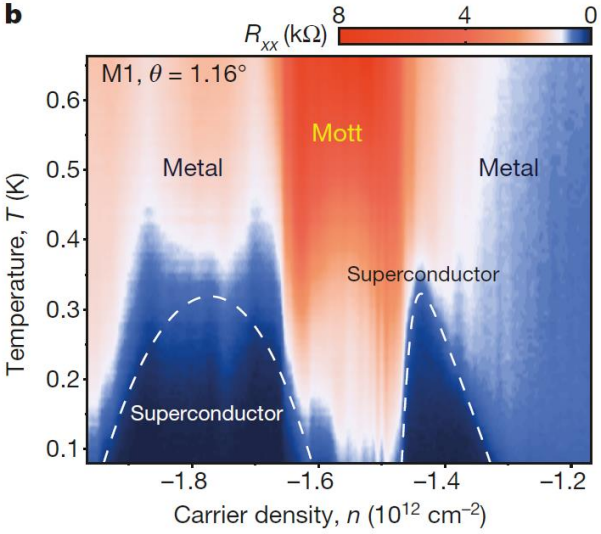

Example: Graphene on hBN

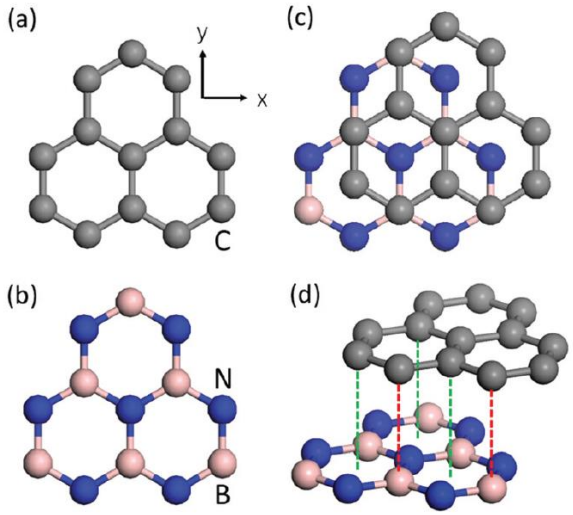

Chen & Qin, JPCC 8, 12085 (2020)

Graphene and hexagonal boron nitride (hBN) have the same crystal structure but slightly different interatomic distances (roughly, 0.142 nm vs 0.145 nm). In hBN they are 1.8% larger

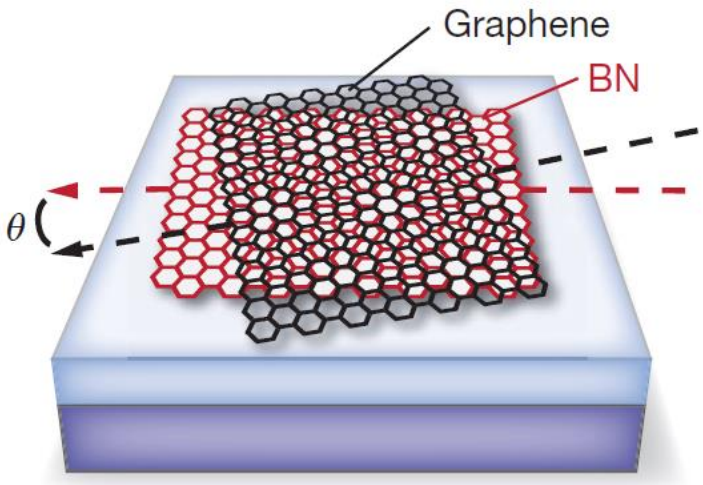

Dean et al, Nature 497, 598 (2013)

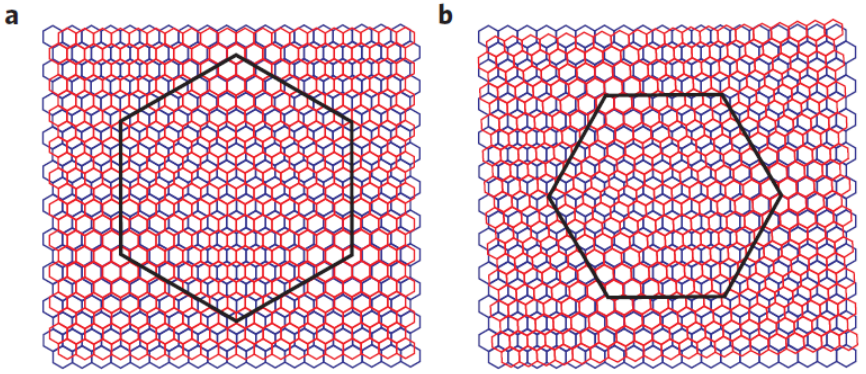

Figure 1 | Schematic representation of the moiré pattern of graphene (red) on hBN (blue). a Relative rotation angle between the crystals $\varphi = 0°$. **b** Relative rotation angle between the crystals $\varphi = 3° \approx 0.052$ rad. The mismatch between the lattices is exaggerated (~10%). Black hexagons mark the moiré plaquette.

Woods et al, Nature Phys. 10, 451 (2014)

Graphene on hBN: Motivation

Graphene at hBN has much higher electron mobility than graphene at any other substrates or freely suspended graphene – why?

Ripples and puddles

Freely suspended graphene has strong thermal fluctuations (intrinsic ripples)

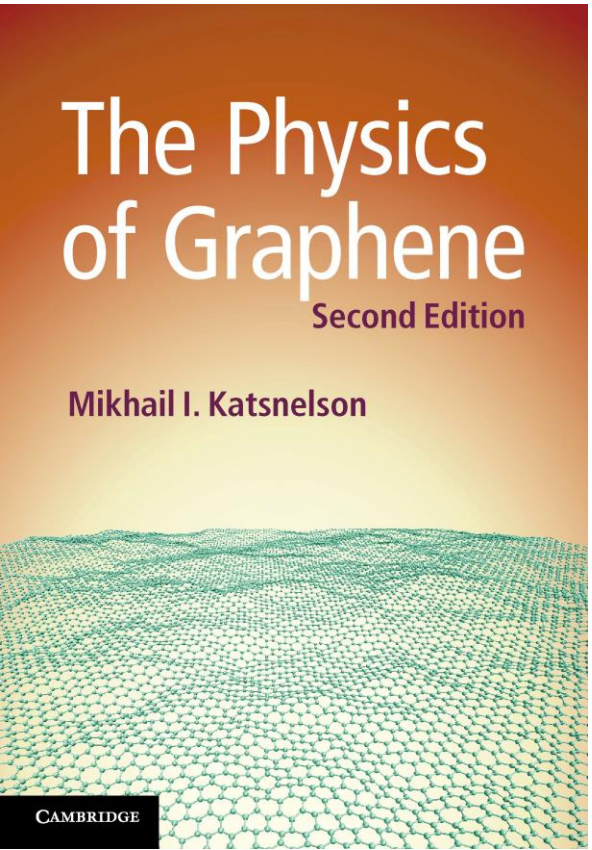

Gibertini, Tomadin, Polini, Fasolino & MIK, PR B81, 125437 (2010)

Atomic displacements at room temperature

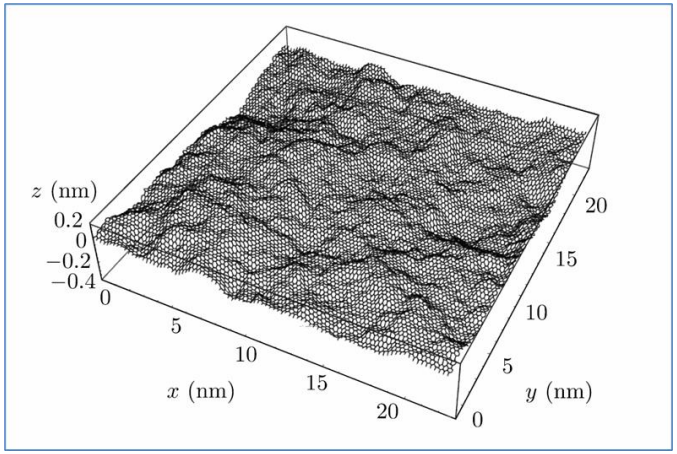

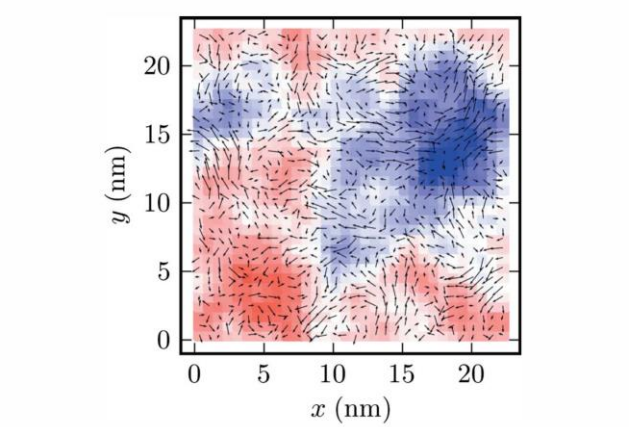

FIG. 2. (Color online) Average displacements $\overline{\boldsymbol{u}}(\boldsymbol{r})$ calculated as discussed in Sec. II A. The color scale represents the $\hat{z}$ component of the average displacements, varying from −3.0 Å (blue) to +3.0 Å (red). The arrows, whose length has been multiplied by a factor ten for better visibility, represent the in-plane components of the average displacements.

Graphene on hBN: Motivation II

Scalar potential

$$V_1 = g_1(u_{xx} + u_{yy})$$

Vector potential

$$V_2 = g_2(u_{xx} - u_{yy} + 2iu_{xy})$$

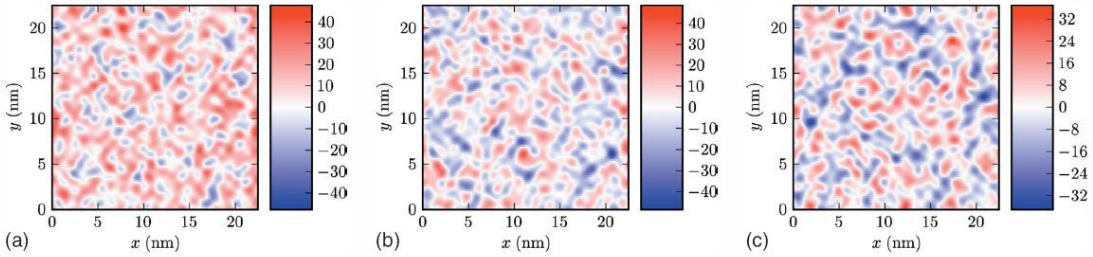

FIG. 3. (Color online) Left panel: color plot of the scalar potential $V_1(\boldsymbol{r})$ (in units of meV) calculated using Eq. (2) with g_1=3 eV. Central panel: the real part of the potential $V_2(\boldsymbol{r})$ (in units of meV) calculated using Eq. (3). Right panel: the imaginary part of the potential $V_2(\boldsymbol{r})$ (in units of meV).

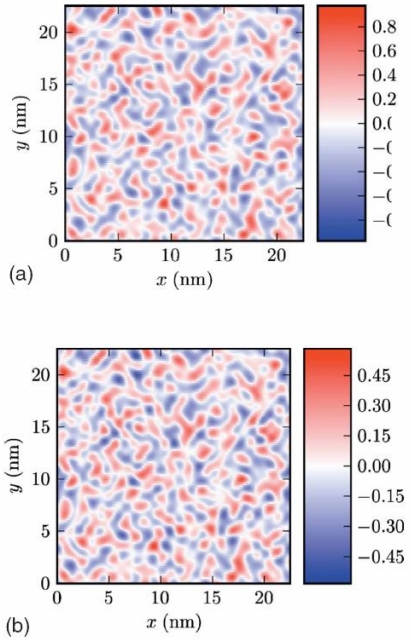

FIG. 4. (Color online) Top panel: fully self-consistent electronic density profile $\delta n(\boldsymbol{r})$ (in units of 10^{12} cm^{-2}) in a corrugated graphene sheet. The data reported in this figure have been obtained by setting g_1=3 eV, α_{ee}=0.9 (this value of α_{ee} is the commonly used value for a graphene sheet on a SiO_2 substrate), and an average carrier density $\bar{n}_c \simeq 0.8 \times 10^{12}$ cm^{-2}. Bottom panel: same as in the top panel but for α_{ee}=2.2 (this value of α_{ee} corresponds to suspended graphene).

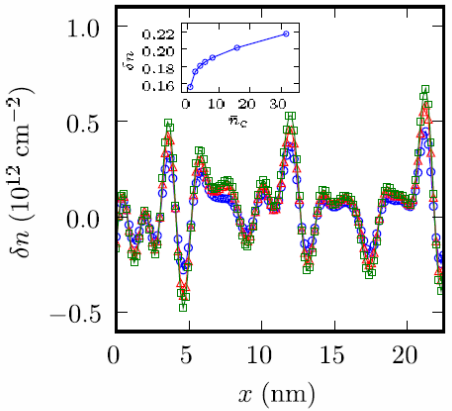

FIG. 9. (Color online) One-dimensional plots of the self-consistent density profiles (as functions of x in nm for y=21.1 nm) for different values of doping: $\bar{n}_c \simeq 0.8 \times 10^{12}$ cm^{-2} (circles), $\bar{n}_c \simeq 3.96 \times 10^{12}$ cm^{-2} (triangles), and $\bar{n}_c \simeq 3.17 \times 10^{13}$ cm^{-2} (squares). The data reported in this figure have been obtained by setting g_1=3 eV and α_{ee}=2.2. The inset shows $\delta n(\boldsymbol{r})$ (in units of 10^{12} cm^{-2}) at a given point $\boldsymbol{r}$ in space as a function of the average carrier density $\bar{n}_c$ (in units of 10^{12} cm^{-2}).

Graphene on hBN: Motivation III

Graphene on SiO_2

Gibertini, Tomadin, Guinea, MIK & Polini PR B 85, 201405 (2012)
Experimental STM data: V.Geringer et al (M.Morgenstern group)

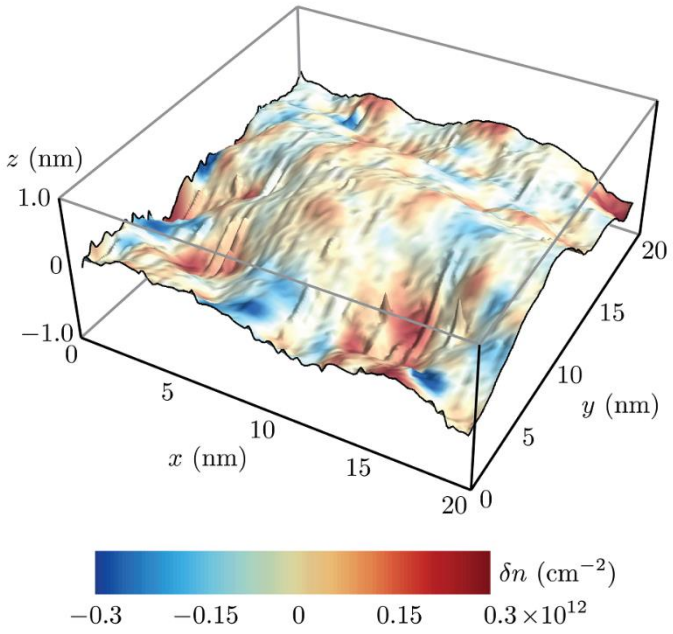

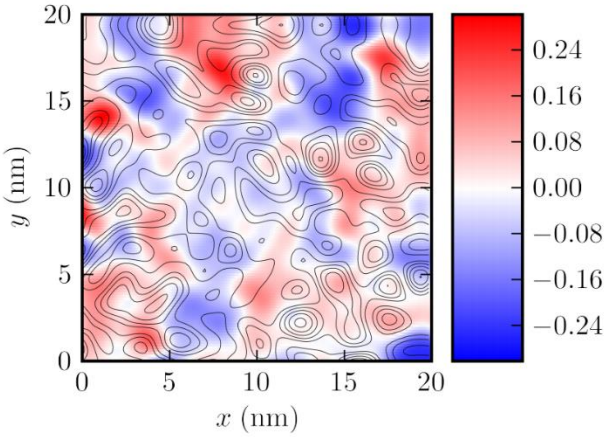

FIG. 3: (Color online) Fully self-consistent induced carrier-density profile $\delta n(\boldsymbol{r})$ (in units of 10^{12} cm^{-2}) in the corrugated graphene sheet shown in Fig. 1. The data reported in this figure have been obtained by setting $g_1 = 3$ eV, $\alpha_{ee} = 0.9$, and an average carrier density $\bar{n}_c \approx 2.5\times10^{11}$ cm^{-2}. The thin solid lines are contour plots of the curvature $\nabla^2_{\boldsymbol{r}} h(\boldsymbol{r})$. Note that there is no simple correspondence between topographic out-of-plane corrugations and carrier-density inhomogeneity.

hBN is atomically flat: suppresses thermal ripples and no ripples due to roughness of substrate

Commensurate-incommensurate transition

Commensurate–incommensurate transition in graphene on hexagonal boron nitride

C. R. Woods[1], L. Britnell[1], A. Eckmann[2], R. S. Ma[3], J. C. Lu[3], H. M. Guo[3], X. Lin[3], G. L. Yu[1], Y. Cao[4], R. V. Gorbachev[4], A. V. Kretinin[1], J. Park[1,5], L. A. Ponomarenko[1], M. I. Katsnelson[6], Yu. N. Gornostyrev[7], K. Watanabe[8], T. Taniguchi[8], C. Casiraghi[2], H-J. Gao[3], A. K. Geim[4] and K. S. Novoselov[1]*

NATURE PHYSICS DOI: 10.1038/NPHYS2954

When misorientation angle (in radians) is smaller with misfit, synchronization happens

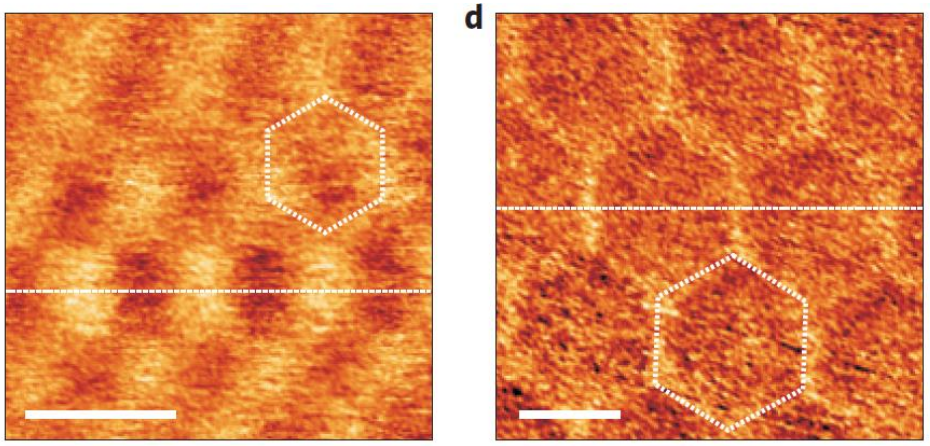

Moire patterns with periodicity 8 nm (left) and 14 nm (right)

Atomistic simulations

PRL 113, 135504 (2014) PHYSICAL REVIEW LETTERS week ending 26 SEPTEMBER 2014

Moiré Patterns as a Probe of Interplanar Interactions for Graphene on h-BN

M. M. van Wijk, A. Schuring, M. I. Katsnelson, and A. Fasolino*

Distribution of bond length in commensurate (left) and incommensurate (right) regimes

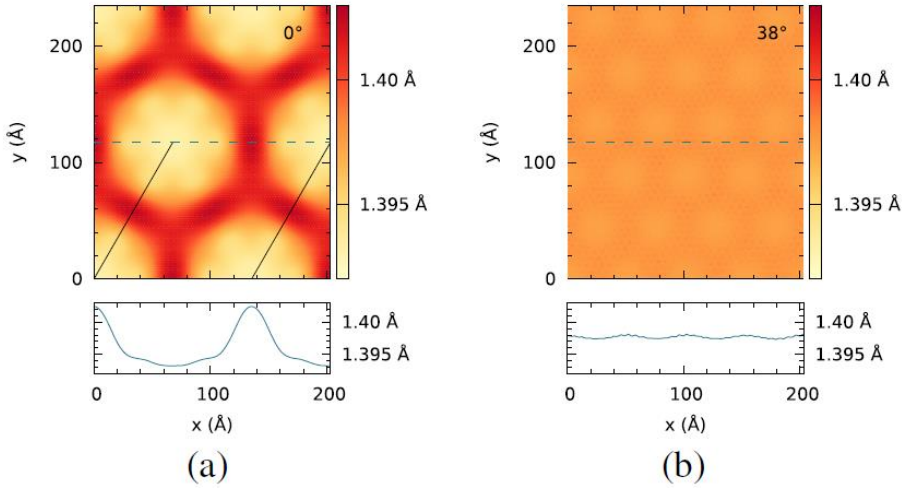

Optimization of structure

PHYSICAL REVIEW B **84**, 195414 (2011)

Adhesion and electronic structure of graphene on hexagonal boron nitride substrates

B. Sachs,[1,*] T. O. Wehling,[1,†] M. I. Katsnelson,[2] and A. I. Lichtenstein[1]

Relaxed structure (B green, C yellow, N red)

V corresponds to the minimal energy (max. cohesion)

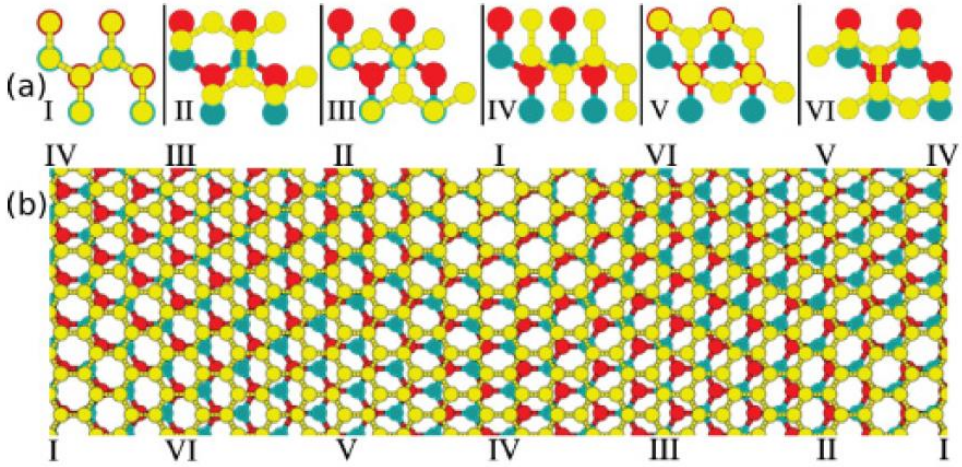

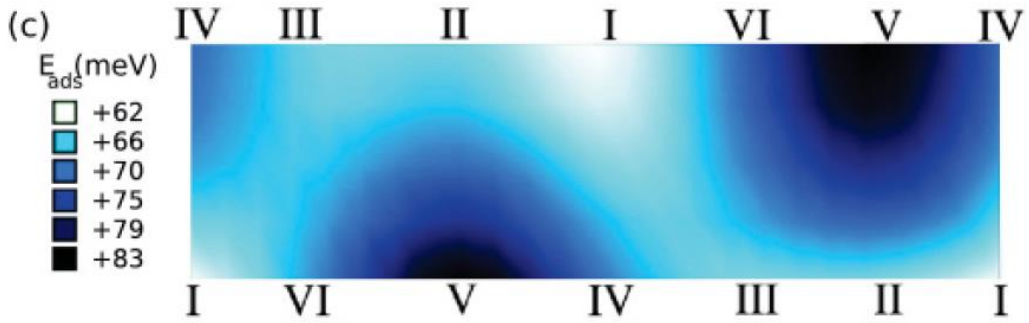

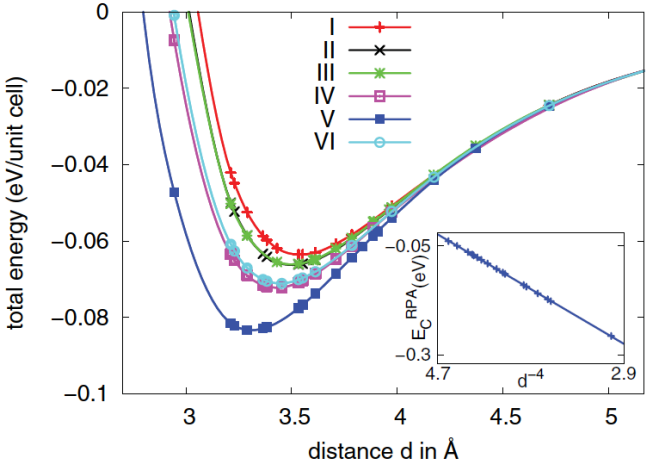

B on the top of C, N in the middle of hexagon

Sublattices are no more equivalent → locally

energy gap is open (mass term in Dirac eq.)

Optical second-harmonic generation

In commensurate phase inversion symmetry in broken due to nonequivalence of sublattices → second-harmonic generation (SHG) is allowed by symmetry

PHYSICAL REVIEW B **99**, 165432 (2019)

Resonant optical second harmonic generation in graphene-based heterostructures

M. Vandelli,[1,2] M. I. Katsnelson,[1,3] and E. A. Stepanov[1,3]

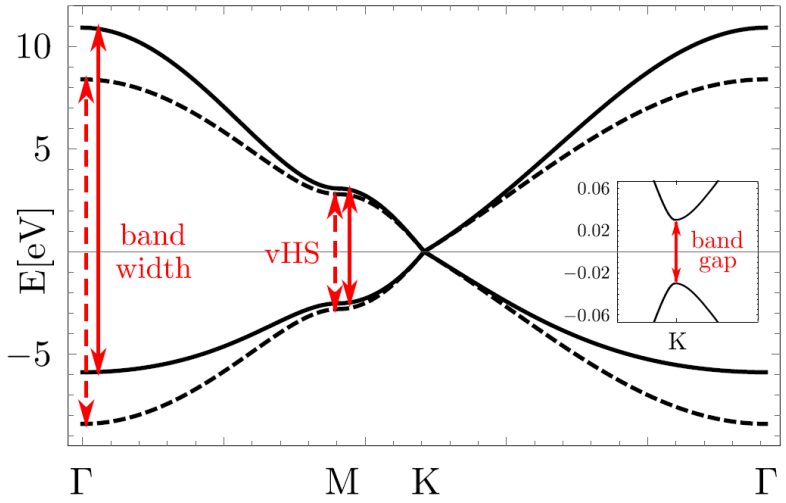

FIG. 1. Dispersion relation of graphene with (solid line) and without (dashed line) account for the next-nearest-neighbor hopping process t'. Red arrows show optical resonances at the bandwidth (Γ point), van Hove singularity (M point), and band gap (K point).

$$t = -2.8 \text{ eV}, t' = -0.1t \quad m = 30 \text{ meV}$$

Electron-hole symmetry should be also broken → either final doping or NNN hopping t'

$$\hat{H}_{ij}[A] = \hat{H}_{ij} \exp\left(-i\frac{e}{c}\int_{\mathbf{R}_i}^{\mathbf{R}_j} \mathbf{A}(\mathbf{r},t)\cdot d\mathbf{r}\right)$$

Contributions to nonlinear optical conductivity

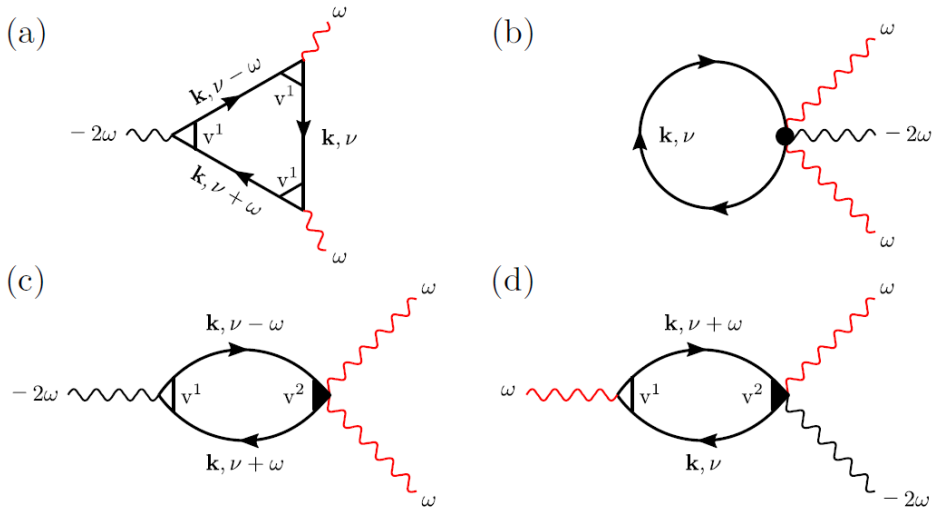

Optical SHG II

Direct Observation of Incommensurate–Commensurate Transition in Graphene-hBN Heterostructures via Optical Second Harmonic Generation

E. A. Stepanov,*,† S. V. Semin,† C. R. Woods, M. Vandelli, A. V. Kimel, K. S. Novoselov, and M. I. Katsnelson

Cite This: *ACS Appl. Mater. Interfaces* 2020, 12, 27758–27764 Read Online

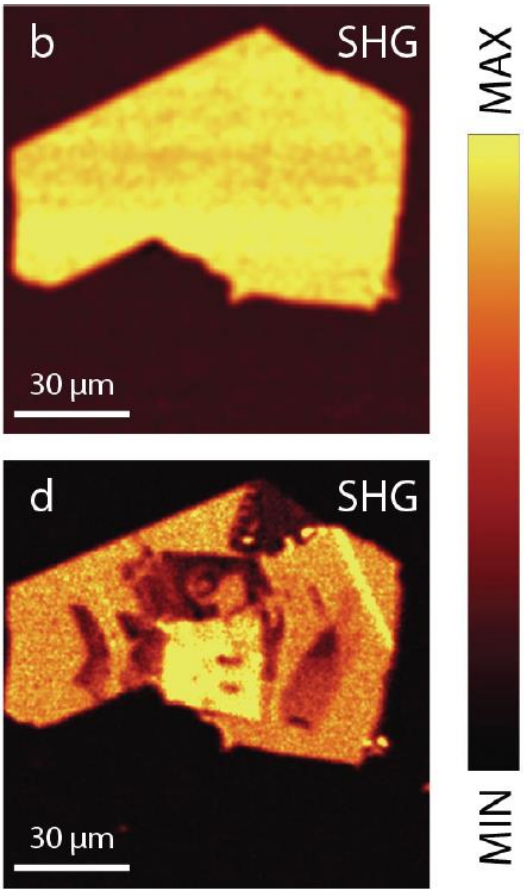

b – incommensurate phase, only hBN signal is visible;
d – commensurate, one can see graphene

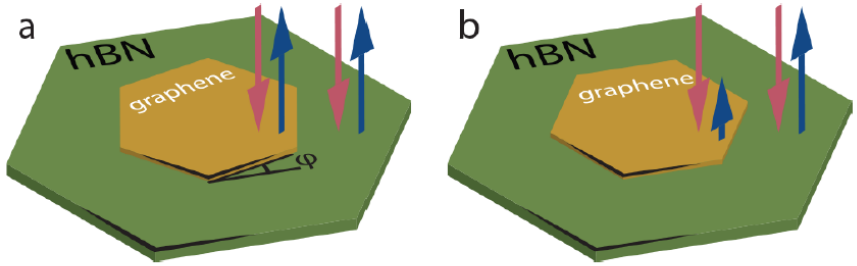

Figure 1. Sketch of the experiment. Green and yellow hexagonal tiles represent hBN and graphene, respectively. Red arrows depict the incident 800 nm light. Blue arrows indicate the SHG response collected at 400 nm from different parts of the sample. (a) In the incommensurate phase, the inversion symmetry of graphene is not broken, and the uniform signal of the SHG comes only from the hBN. (b) After the structural phase transition to the commensurate state, strong modification of the SHG response is observed from the graphene area, where the inversion symmetry breaking is induced by the aligned hBN substrate.

Commensurate – incommensurate transition was induced by heating and clearly detected via SHG

Graphene on graphite

Relaxation of moiré patterns for slightly misaligned identical lattices: graphene on graphite

2D Mater. **2** (2015) 034010

M M van Wijk, A Schuring, M I Katsnelson and A Fasolino

Atomistic simulations: graphene on graphite

Periodicity of moire structure $a_m = \dfrac{a_{\text{lattice}}}{2|\sin(\theta/2)|}$

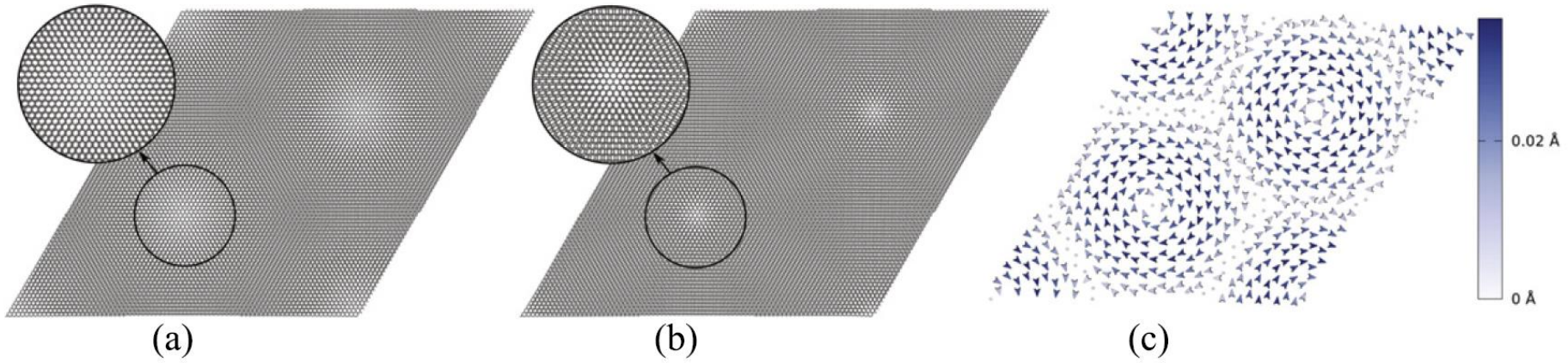

Figure 2. The effects of relaxation are shown for a sample with $(n, m) = (82,1)$, $\theta = 1.2°$ and $a_m = 115.3$ Å. (a) The sample prior to relaxation, (b) the sample after relaxation. Notice the shrinking of the AA stacked area. (c) The displacements of the atoms as the result of relaxation for a sample $(n, m) = (17,1)$, $\theta = 5.7°$ and $a_m = 24.5$ Å. The colour indicates size and the arrow the direction of the displacements.

Graphene on graphite II

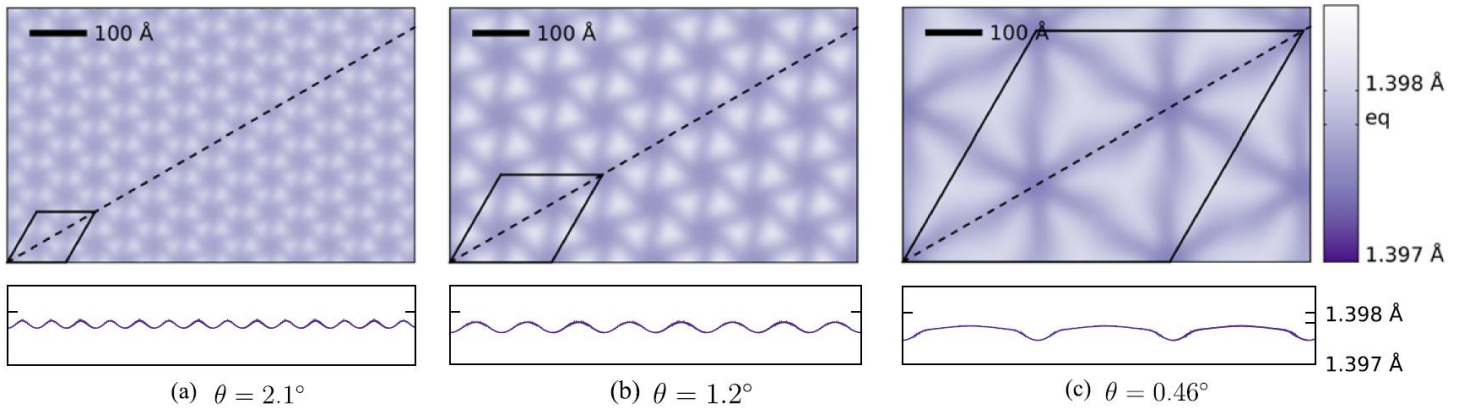

Figure 4. Bond lengths of relaxed configurations for samples where the graphene layer is relaxed in all directions. The supercell is shown in black. The bottom panels show the bond length along the dashed diagonal line. (a) $\theta = 2.1°$, $(n, m) = (47,1)$, $a_m = 66.4$ Å. (b) $\theta = 1.2°$, $(n, m) = (82,1)$, $a_m = 115.3$ Å. (c) θ=0.46°, $(n, m) = (216,1)$, $a_m = 302.6$ Å.

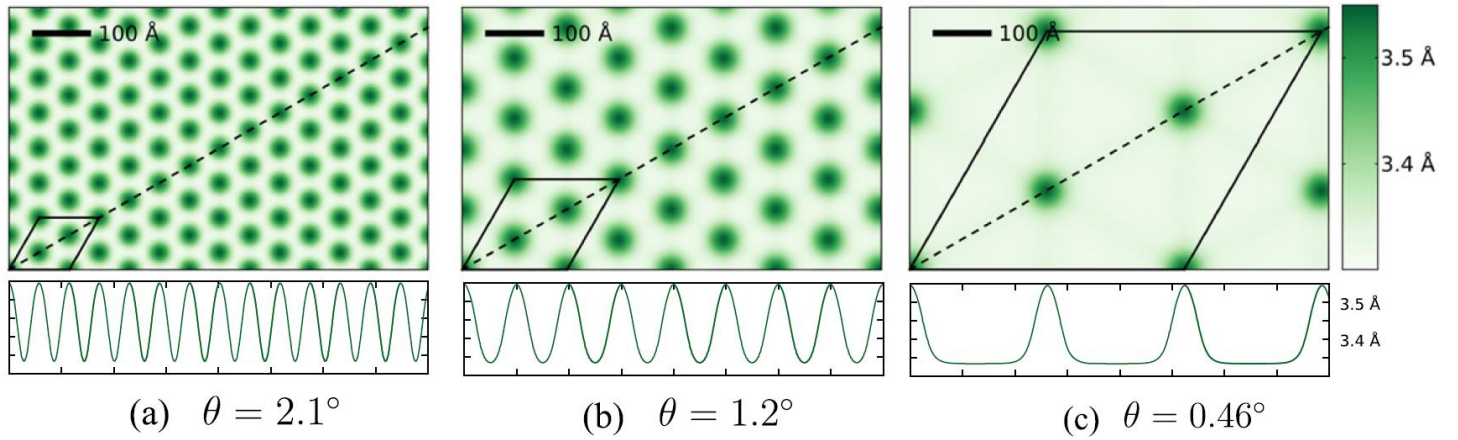

Figure 6. Out-of-plane distance for samples where the graphene layer is relaxed in all dimensions. The bottom panels show the out-of-plane distance along the dashed diagonal line. (a) $\theta = 2.1°$, $(n, m) = (47,1)$, $a_m = 66.4$ Å. (b) $\theta = 1.2°$, $(n, m) = (82,1)$, $a_m = 115.3$ Å. (c) $\theta = 0.46°$, $(n, m) = (216,1)$, $a_m = 302.6$ Å.

Twisted bilayer graphene

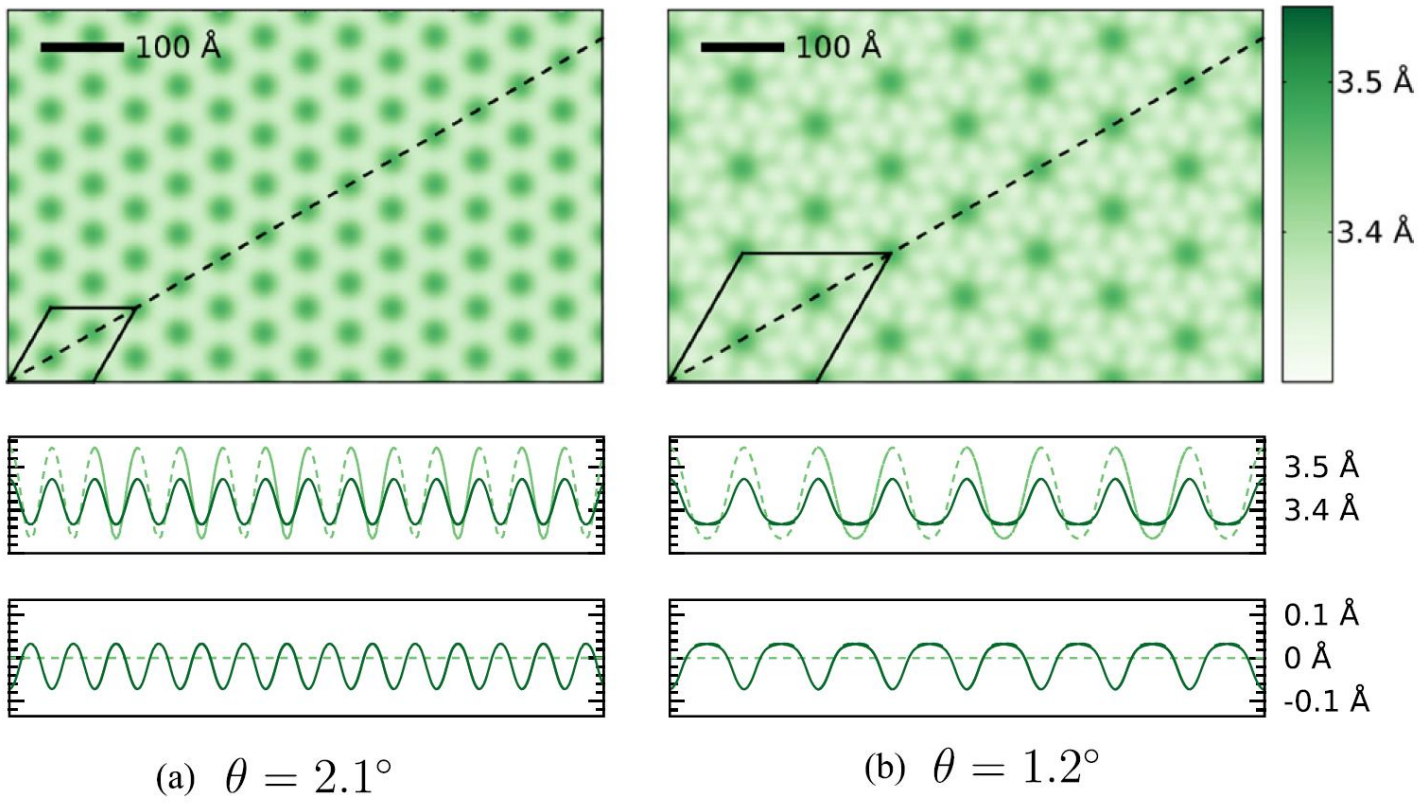

Figure 8. Out-of-plane distance for double layer graphene. The bottom four panels show z along the dashed line in the top figure. The dashed lines show the z for graphene on graphite as in figure 6.

There is a modulation at small angles and some analog of "incommensurability" (small modulations) at larger angles

Messages to take home

- Sometimes it is not enough to consider generic case, (accidental) degeneracy can dramatically change the physics, and it happens

Fermi resonance plays a role in properties of water and many organic substances (containing C-H bond like in benzene molecule)

- Close to the resonance there is phase synchronization and energy transfer between modes in the resonance

- Synchronization in space (commensurate-incommensurate transition) is a very hot subject now, e.g. for Van der Waals heterostructures

THANK YOU